

Research Paper

A smart bilayered scaffold supporting keratinocytes and muscle cells in micro/nano-scale for urethral reconstruction

XiangGuo Lv^{1*}, Chao Feng^{2*}, YiDong Liu^{1*}, XuFeng Peng², ShiYan Chen³, DongDong Xiao¹, HuaPing Wang³, Zhe Li⁴✉, YueMin Xu²✉, MuJun Lu¹✉

1. Department of Urology and Andrology, Shanghai Renji Hospital, Shanghai Jiao Tong University, School of Medicine, Shanghai, China;
2. Department of Urology, Shanghai Jiao Tong University Affiliated Sixth People's Hospital, Shanghai, China;
3. State Key Laboratory for Modification of Chemical Fibers and Polymer Materials, College of Materials Science and Engineering, Donghua University, Shanghai, China;
4. College of Materials and Textile Engineering, JiaXing University, Zhejiang, China.

*Co-first author: These authors contributed equally to the work

✉ Corresponding author: MuJun Lu MD. PhD; E-mail: lumujun@163.com; Zhe Li PhD; E-mail: lizhe830817@163.com; YueMin Xu MD. PhD; E-mail: xuyuemin@263.net

© Ivyspring International Publisher. This is an open access article distributed under the terms of the Creative Commons Attribution (CC BY-NC) license (<https://creativecommons.org/licenses/by-nc/4.0/>). See <http://ivyspring.com/terms> for full terms and conditions.

Received: 2017.07.25; Accepted: 2018.01.30; Published: 2018.05.09

Abstract

Rationale: In urethral tissue engineering, the currently available reconstructive procedures are insufficient due to a lack of appropriate scaffolds that would support the needs of various cell types. To address this problem, we developed a bilayer scaffold comprising a microporous network of silk fibroin (SF) and a nanoporous bacterial cellulose (BC) scaffold and evaluated its feasibility and potential for long-segment urethral regeneration in a dog model.

Methods: The freeze-drying and self-assembling method was used to fabricate the bilayer scaffold by stationary cultivation *G. xylinus* using SF scaffold as a template. The surface morphology, porosity and mechanical properties of all prepared SF-BC scaffolds were characterized using Scanning electron microscopy (SEM), microcomputed tomography and universal testing machine. To further investigate the suitability of the bilayer scaffolds for tissue engineering applications, biocompatibility was assessed using an MTT assay. The cell distribution, viability and morphology were evaluated by seeding epithelial cells and muscle cells on the scaffolds, using the 3D laser scanning confocal microscopy, and SEM. The effects of urethral reconstruction with SF-BC bilayer scaffold was evaluated in dog urethral defect models.

Results: Scanning electron microscopy revealed that SF-BC scaffold had a clear bilayer structure. The SF-BC bilayer scaffold is highly porous with a porosity of 85%. The average pore diameter of the porous layer in the bilayer SF-BC composites was $210.2 \pm 117.8 \mu\text{m}$. Cultures established with lingual keratinocytes and lingual muscle cells confirmed the suitability of the SF-BC structures to support cell adhesion and proliferation. In addition, SEM demonstrated the ability of cells to attach to scaffold surfaces and the biocompatibility of the matrices with cells. At 3 months after implantation, urethra reconstructed with the SF-BC scaffold seeded with keratinocytes and muscle cells displayed superior structure compared to those with only SF-BC scaffold.

Principal Conclusion: These results demonstrate that the bilayer SF-BC scaffold may be a promising biomaterial with good biocompatibility for urethral regeneration and could be used for numerous other types of hollow-organ tissue engineering grafts, including vascular, bladder, ureteral, bowel, and intestinal.

Key words: bilayer scaffold, bacterial cellulose, silk fibroin, urethral reconstruction, lingual keratinocytes, muscle cells

Introduction

Several congenital and acquired pathologies, including hypospadias, epispadias, strictures, fistulas, malignancy, and straddle injuries, can compromise

the normal functionality of the urethra and require urethral reconstruction [1]. End-to-end anastomosis is frequently used to repair short, non-complex urethral

defects, but reconstruction of long-segment urethral strictures remains a challenging problem in urology. Bladder mucosa, oral mucosa, and colonic mucosa have been used for long-segment urethroplasty [2-4]. However, harvesting complications, such as submucosal scarring, pain, numbness, injury to salivary ducts and limitation of mandibular movement, have been reported [5].

Tissue engineering approaches provide potential strategies for developing biological substitutes to restore and maintain the normal functional anatomy of the urethra [6, 7]. Over the past several decades, decellularized matrixes, such as small intestinal submucosa (SIS) [8] and the bladder acellular matrix (BAM) [9], as well as synthetic polymeric materials, including polylactic acid (PLA) [10] and polylactic-co-glycolic acid (PLGA) [11], either alone or seeded with cells, have been successfully used for urethral reconstruction. However, long-term adverse effects of decellularized matrixes and synthetic polymeric materials have been reported, such as stricture recurrence, fistula formation and foreign body responses [12-14]. It is known that urine leakage plays an important role in scarring and fistula formation [8]; so, a scaffold architecture with a barrier function against urine could be a direction for urethral biomaterials. Therefore, further refinements are required to overcome the limitations of biomaterials for urinary tract reconstruction.

In urethral tissue engineering, designing biomaterials that mimic the native structure of the urethral extracellular matrix (ECM) could be a promising approach. The structure of the urethra consists of two major layers: the stratified epithelium and the organized subcutaneous layer. The epithelium-laden epidermis is the upper, thin layer that functions as the barrier of the urethra. The lower, subcutaneous layer, which is thicker, contains muscle cells and fibroblast cells and provides strength and flexibility [15]. This complex structure makes urethral engineering challenging. In addition to the cells, the bilayer scaffolds intended for use in urethral applications is composed of an upper, smooth layer and a porous or sponge-like sublayer, which could fulfill the specific requirements of the three-dimensional (3D) architecture, the microenvironmental needs of the various cell types of the urethra, and provide a diffusion barrier function and structural integrity.

In order to achieve this kind of structure, Eberli et al. described the fabrication of a bilayer scaffold by suturing a collagen matrix to polyglycolic acid (PGA) polymer with collagen-threaded stitches [16]. However, the suturing of polymers may compromise the barrier function of the scaffold, which is

indispensable for hollow organ reconstruction. We previously fabricated bacterial cellulose (BC), a biodegradable polymer produced by *Gluconacetobacter xylinus* [17]. BC combines the important and well-known qualities of cellulose with the outstanding features of nano-scale materials [18]. There is much interest in the development of medical applications based on BC for wound care, such as modern wound dressings and artificial skins [19], and implantable tissue engineered biomaterials, such as blood vessels [20] and bone [21]. In particular, the nanofibrous network architecture of BC mimics the extracellular matrix (ECM), which may have significant effects on cell adhesion and proliferation in tissue engineering [22]. However, BC itself lacks a microporous architecture. The relatively dense nanostructure of the nanofibrous network allows only limited cell migration, penetration and ingrowth. Our previous studies have shown that silk fibroin, derived from silkworms, is a promising bioscaffold in regenerative medicine owing to its favorable properties, such as high structural strength and elasticity, low antigenicity, and easily controllable 3D fibrous scaffolds [23-25]. Silk fibroin scaffolds have suitable cytocompatibility and supported the formation of smooth muscle and urothelial tissues in dog models of urethral reconstruction. Therefore, in the current study, we developed a bilayer scaffold comprising a microporous network of silk fibroin (SF), which allows ingrowth of surrounding host tissues, and a nanoporous surface of bacterial cellulose (BC), which provides a fluid-tight seal for retention of urine, and evaluated its feasibility and potential *in vitro* and *in vivo*.

Another critical factor in generating tissue-engineered urethral tissue for patients is the cell source. Typically, epithelial cells and muscle cells are used to construct urethral tissue. Cells obtained from bladder biopsies are a main source for a cell-based tissue-engineered (TE) urethra [26]. However, healthy cells might not be available in patients with chronic inflammation due to a urinary tract infection or an indwelling catheter. Lingual mucosa is considered the ideal tissue for urethral reconstruction [27], and a previous study demonstrated that lingual keratinocytes and muscle cells can be collected from the lingual mucosa and used as a source of seed cells for urethral tissue engineering [28]. Thus, in the present study, we cultured autologous lingual keratinocytes and muscle cells and then seeded them onto a SF-BC scaffold with a 3D microporous/nanoporous structure to obtain a new type of 3D urethral tissue for urethral reconstruction.

Methods

Fabrication of the bilayer SF-BC scaffolds

All chemicals were purchased from Sinopharm Chemical Reagent Co., Ltd. (Shanghai, China). *Gluconacetobacter xylinus* strain 1.1812 was obtained from the Institute of Microbiology, Chinese Academy of Science. The culture medium for *Gluconacetobacter xylinus* consisted of 5.0 wt% D-glucose, 0.5 wt% peptone, 0.5 wt% yeast extract, 0.2 wt% disodium hydrogen phosphate, 0.1 wt% monopotassium phosphate and 0.1 wt% citric acid, and the pH was adjusted to 5.0 with NaOH. The medium was sterilized at 121°C in an autoclave for 30 min.

The bilayer SF-BC scaffold was composed of 3-D microporous SF and BC. Preparation of the silk fibroin solution followed a procedure described previously [29, 30]. Next, the prepared SF solution (2% w/v) was slowly poured into a vessel, which was then transferred to the refrigerator and frozen at -80°C for 24 days. The frozen protein samples were lyophilized for 24 h to prepare a 3-D microporous SF and stored at 4°C until further use.

To fabricate the nanoporous surface, we first treated the 3-D microporous SF with 70% (v/v) ethanol for 30 min to induce crystallization and insolubility in water. Then, the scaffolds were repeatedly washed with sterile culture medium to remove any remaining alcohol. The culture medium, containing *Gluconacetobacter xylinus* at an initial bacterial density of 3.8×10^7 cells/ml, was added in a culture vessel to a depth of 1 mm. The 3-D porous SF scaffolds were placed in the culture vessel. Then, the medium was incubated statically at 30°C for 3 days to produce the SF-BC scaffolds. To further purify the scaffolds, the composites were immersed in 75 wt% ethyl alcohol for 24 h, then treated with 1 wt% Triton X-100 in ultrapure water for 24 h, after which they were rinsed with ultrapure water 3 times to remove the excess chemical. Unmodified BC was prepared for comparison. The samples were cut into fixed sizes (i.e., 10 cm × 3 cm) and freeze-dried at -20°C for 24 h for further characterization.

Scanning electron microscopy

The surface morphology of all prepared SF-BC scaffolds was characterized using an S-4800 FE SEM operated at 10 kV. Prior to analysis, small pieces were cut from the freeze-dried samples and coated with a thin layer of sputtered gold. The average fiber diameter was measured using Image J through the analysis of SEM images; at least 100 fibers and 100 pores were assessed.

Porosity measurements

The porosity of the scaffold sections was measured using microcomputed tomography (Micro-CT) (Skyscan 1272, Bruker). Briefly, scaffold samples underwent Micro-CT in order to evaluate the pore structures of those scaffolds. After scanning, the pore size, porosity and connectivity of the films were analyzed by the CTAn program (Skyscan Company).

Measurement of mechanical properties

The tensile strength of the SF-BC scaffolds (n=5) was measured using a universal testing machine (Instron 5969, Instron, USA) at room temperature with a crosshead speed of 2 mm/min. Before testing, all scaffolds were rehydrated in phosphate-buffered saline (PBS) solution for 30 min. The Young's modulus and stress and strain at break were determined using the manufacturers' software. Briefly, 5 mm length strips were clamped at each end by metal clips. Using the manufacturer's software, the Young's modulus was calculated from the slope of the initial linear section of the stress-strain curve. Stress at break and strain at break ($L_b/L_0 \times 100\%$, where L_0 is the initial length of the sample and L_b is the sample length at break time) were determined.

The suture-retention strength was measured using the instrument and a suture (Polyglactin 910, 5-0 size, Ethicon Inc.). Briefly, the SF-BC scaffolds were fixed in the lower grip of the instrument and a suture was inserted 2 mm from its outside edge. The two ends of the suture were attached to the upper grip and pulled at a constant rate of 1 mm/min. The suture-retention strength was defined as the peak force obtained during this procedure.

Cell isolation and expansion

Healthy female beagle dogs (averaging 1.1 y, 11.5 kg) were used in this study. A 0.3 cm × 0.3 cm section of lingual tissue was harvested using a biopsy punch (Kai Industries, Gifu, Japan) from healthy dog lingual tissue and the wound was sutured. The tissue was then divided into mucosal and muscle sections using a sterile scalpel. The cell culture methods were reported previously [31]. Briefly, muscle tissues were minced and digested with 0.5 wt% type I collagenase (Worthington, USA). After 30 min, the suspended cells were filtered through a 74 μm cell strainer and then cultured in high glucose Dulbecco's modified Eagle's medium (DMEM) supplemented with 10% fetal bovine serum (FBS). The mucosal sections were incubated in dispase II (Roche) overnight at 4°C. Then, a thin epithelial layer was peeled from the submucosa and treated with 0.05% trypsin (Gibco). The suspended cells were cultured in keratinocyte serum-free medium (KFSM; Gibco). The lingual

keratinocytes were identified using immunohistochemical (IHC) staining with antibody AE1/AE3 (Abcam). The lingual muscle cells were identified using an anti-desmin antibody (Abcam).

Scaffold cytotoxicity assay

To detect cytotoxicity of the scaffold, a cell-proliferation assay was performed *in vitro* as described in a previous study [32]. Briefly, 1 mL of cell suspension (lingual keratinocytes and muscle cells) at a density of 10^4 cells/mL was seeded into a 24-well plate. The cells were allowed to adhere for 4 h. The medium with non-adherent cells was removed, and medium containing SF-BC was added. A control without scaffolds was also carried out. The cellular growth at 1, 3, 5, 7 and 9 days of incubation was evaluated by the MTT (3-(4,5-dimethylthiazol-2-yl)-2,5-diphenyl-tetrazolium bromide) assay, a colorimetric test (optical density, OD value) that measures mitochondrial activity.

In vitro incubation of engineered urethral tissue

Before cell seeding, the final SF-BC scaffolds were sterilized with 75% ethanol for 2 h, washed three times in sterilized PBS and then filled with 5 mL of DMEM with 10% FBS for 24 h at 37°C. The lingual muscle cells (5×10^6 cells) were first seeded onto the porous layer of the SF-BC composite scaffold (2×5 cm) and then cultured in DMEM containing 10% FBS. Four days later, the lingual keratinocytes (5×10^5 cells) were seeded onto the dense layer and cultured in a medium composed of KSFM and DMEM (1:1). The compound scaffold was incubated under static conditions for an additional 4 days under an air-fluid level at 37°C in a humidified atmosphere with 5% CO₂. The medium was changed daily.

To further assess the cellular distribution and infiltration within the scaffold, an immunofluorescence assay was performed. The epithelial cell layers were identified using the AE1/AE3 antibody. Muscle cells were identified using an anti-desmin antibody. The nuclei in the sections were stained with 4',6-diamidino-2-phenylindole (DAPI) (Abcam, USA) [31]. The images were captured using a confocal laser-scanning microscope (Carl Zeiss, LSM710).

Cell adhesion on scaffolds was imaged using SEM. SF-BC composites containing muscle cells and keratinocytes were fixed with 2.5% glutaraldehyde for >3 h. The substrates were dehydrated in 50%, 60%, 70%, 80%, 90%, 95%, and 100% ethanol and dried in butyl alcohol. Samples were mounted onto SEM stubs, sputter-coated with gold and imaged by SEM (S-4800 FE)

Surgical procedure for urethral reconstruction and follow-up

For the animal experiments, 20 female beagle dogs (averaging 1.1 y, 11.5 kg) were divided into two groups of 10 dogs each. Group A was given SF-BC scaffolds seeded with keratinocytes and muscle cells, and group B was given SF-BC scaffolds. All dogs were anesthetized with pentobarbital. The urethra between the bladder and the pubic symphysis was exposed, and a 5 cm long segment was transected and removed (Fig. 5 A). Then, the SF-BC scaffold was tubularized by suturing an 8F urethral catheter in preparation for urethroplasty (Fig. 5 C,D). Urethral repair was performed with 5-0 vicryl sutures applied in interrupted suturing (Fig. 5 E). The new urethra and its anastomosis were covered by the omentum majus for preventing anastomotic leakages and strictures with 5-0 vicryl sutures applied in continuous suturing (Fig. 5 F). Multiple non-absorbable marking sutures were placed at anastomotic margins. The catheter remained in place for 14 days after operation. After the urethral caliber was assessed with retrograde urethrograms, five animals from each group were killed at one and three months post-implantation. The entire urethra was removed, prepared by H&E/Masson staining and assessed by viewing sections of tissue in the mucosal membrane. In Masson staining, the collagen fibers, mucus and cartilage are blue; the cytoplasm, muscle, cellulose, and glia are red, and cell nuclei are black-blue. Immunohistochemical (IHC) staining was performed using monoclonal antibodies against cytokeratin (AE1/AE3; Abcam, Cambridge, Britain), α -smooth muscle actin (α -SMA; Santa Cruz Biotech), and vascular CD31 (CD31; Santa Cruz Biotech) for detecting the epithelial cells, smooth muscle cells, and blood vessels, respectively.

Ethical approval and informed consent

The entire animal experimental protocol was approved by the Animal Care and Use Committee of Shanghai Jiao Tong University Affiliated Sixth People's Hospital before study initiation. All the methods were carried out in accordance with the approved guidelines.

Statistical analysis

All data are expressed as mean \pm standard deviation. ANOVA was used to determine differences between two groups using SPSS17.0 statistical software. Differences were considered statistically significant when the P-value was < 0.05.

Results

Schematic of the biosynthesis of SF-BC composites

Fig. 1 is a schematic illustration of the biosynthesis of the SF-BC composites. First, the 3-D porous SF scaffold was formed using freeze-drying techniques. After inoculation, the bacterial cells synthesized cellulose nanofibrils as they migrated in the porous SF scaffold to gradually form a dense cellulose network at the nanoscale. The SF-BC composites, which consist of nanofibrous BC and porous SF, have a clear bilayer structure with a smooth upper layer and a porous lower layer. Oral tissue was harvested from female dogs by punch biopsy and divided into muscle sections. Muscle cells and keratinocytes were seeded onto the SF-BC composites. Then, the cell-seeded composite sheets were tubularized to complete the TE urethra, which was autologously grafted to surgically induced urethral defects.

Macro- and micro-morphology observations and porosity measurements of SF-BC composites

After seven days of static culture, the SF-BC scaffolds had a clear bilayer structure. The yellow SF layer remained dominant, and a thin white BC film covered the porous SF layer, as observed in the images (Fig. 2 A, B).

As shown in the Table 1, the SF-BC bilayer scaffold is highly porous with a porosity of 85%. The average pore diameter of the porous layer in the bilayer SF-BC composites was 210.2 μm (Fig. 2 F,

G, H).

The surface morphology was further investigated using SEM (Fig. 2 C, D, E). As a result of the random movement of bacteria near the oxygen-rich region during static culture, the isotropic cellulose fiber network is characteristic of dense layered structures. The average nanofiber diameters of BC were approximately 47 nm and could be observed at a high magnification.

Mechanical properties

The mechanical strength of wet SF-BC scaffolds was assessed to determine the material's ability to withstand the stresses during handling and implantation. The results of mechanical testing are presented in Table 2. The suture-retention strength of the scaffold was 1.45 ± 0.21 N, and the Young's modulus was 6.85 ± 0.26 MPa.

Cytotoxicity results

The lingual keratinocytes and muscle cells grew well in the medium containing SF-BC, and the OD values in the scaffold groups were similar to those in the control group (Fig. 3 A, B; $p > 0.05$).

In vitro incubation of engineered urethral tissue

After incubation, the lingual keratinocytes had a typical cobblestone-like appearance, and immunofluorescence staining was positive for AE1/AE3 (Abcam, USA) (Fig. 4 A). The lingual muscle cells exhibited a typical phenotype, and immunofluorescence staining demonstrated that these cells were positive for desmin antibodies (Abcam, USA) (Fig. 4 C).

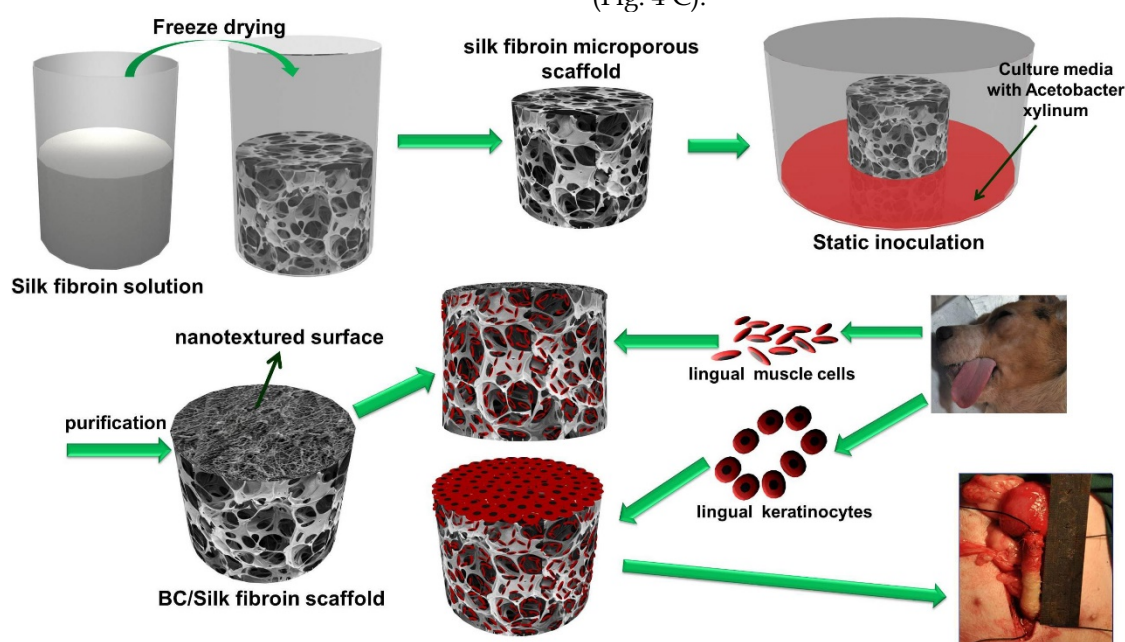


Figure 1. Schematic illustration of the biosynthesis of bilayer SF-BC composites and the experimental design to fabricate TE urethra.

Table 1 The medium thickness, porosity, pore size and the nanofiber diameter of the SF-BC bilayer scaffold.

Bilayer scaffold thickness	Porosity	Nanofiber diameter of nanotextured surface	Pore size of microporous scaffold
4.4±0.52 mm	85±5.8 %	46.7±6.7 nm	210.2±117.8 μm

Table 2 The Young's modulus, stress and strain at break and suture-retention strength of SF-BC bilayer scaffold.

Sample code	Stress at break (KPa)	Strain at break (%)	Young's modulus (MPa)	Suture retention strength (N)
SF-BC	274.6±15.4	15.7±1.4	6.85±0.26	1.45±0.21

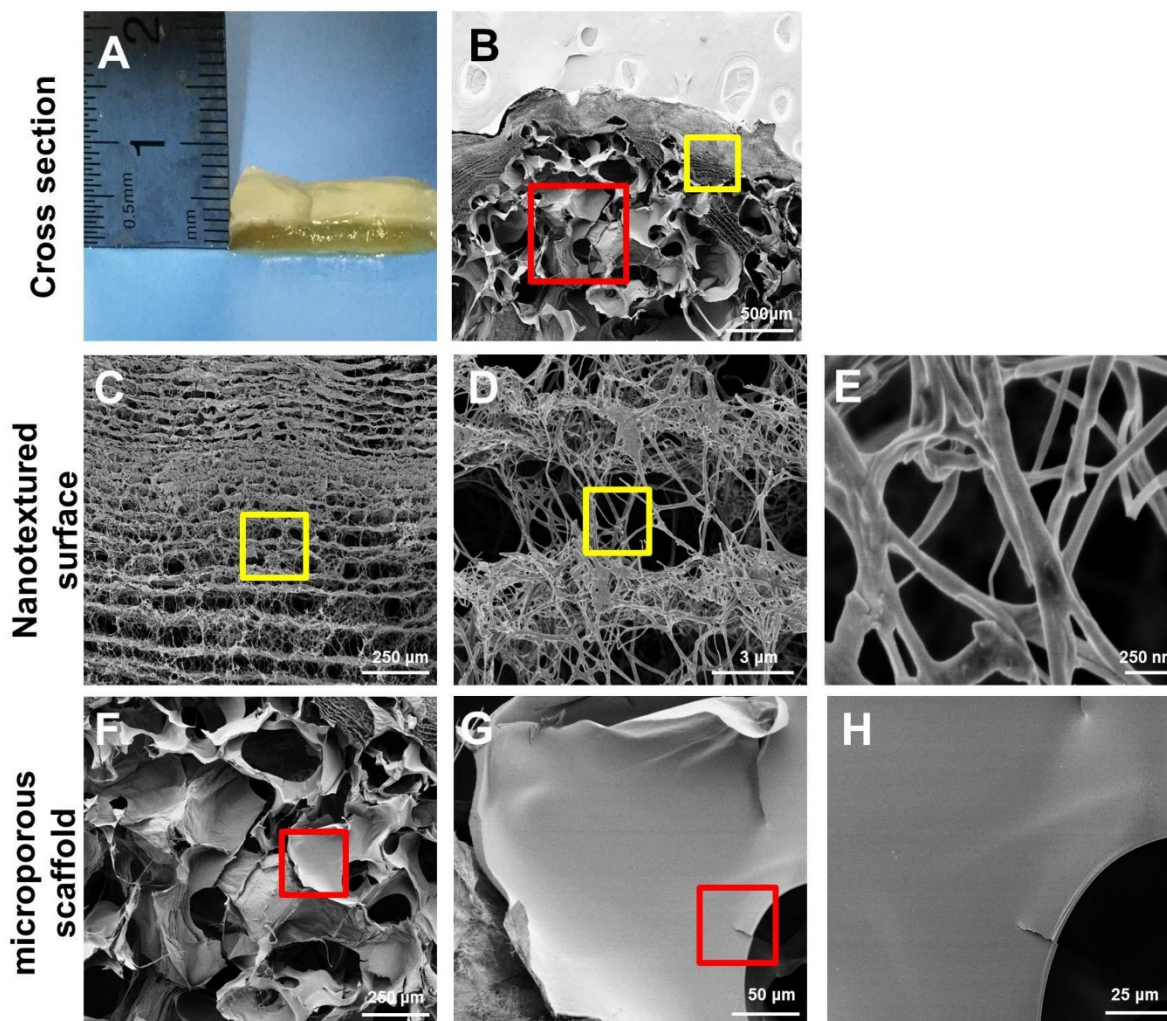


Figure 2. Structural and mechanical analyses of the SF-BC scaffold. (A) Digital photographs of the SF-BC scaffold. (B) Cross-sectional scanning electron microscopy (SEM) images of the SF-BC scaffold. (C-E) Representative SEM images of the architectures in the dense layer. (F-H) Representative SEM images of the architectures in the porous layer.

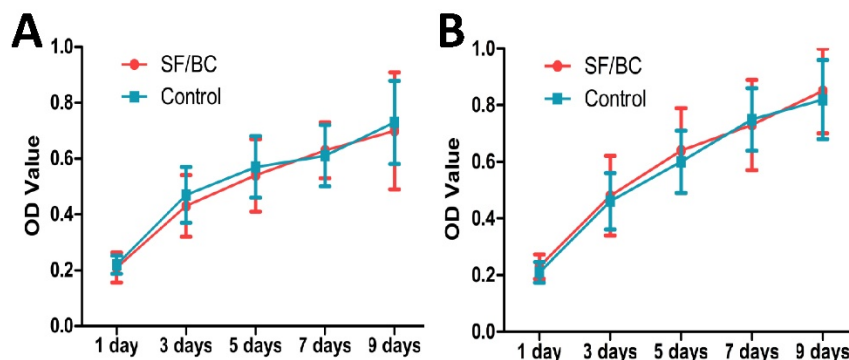


Figure 3. (A) MTT results from proliferation assays using lingual keratinocytes. (B) MTT results from proliferation assays using lingual muscle cells. The lingual keratinocytes and muscle cells grew well in the medium containing SF-BC, and the OD values in the scaffold groups were similar to those in the control group.

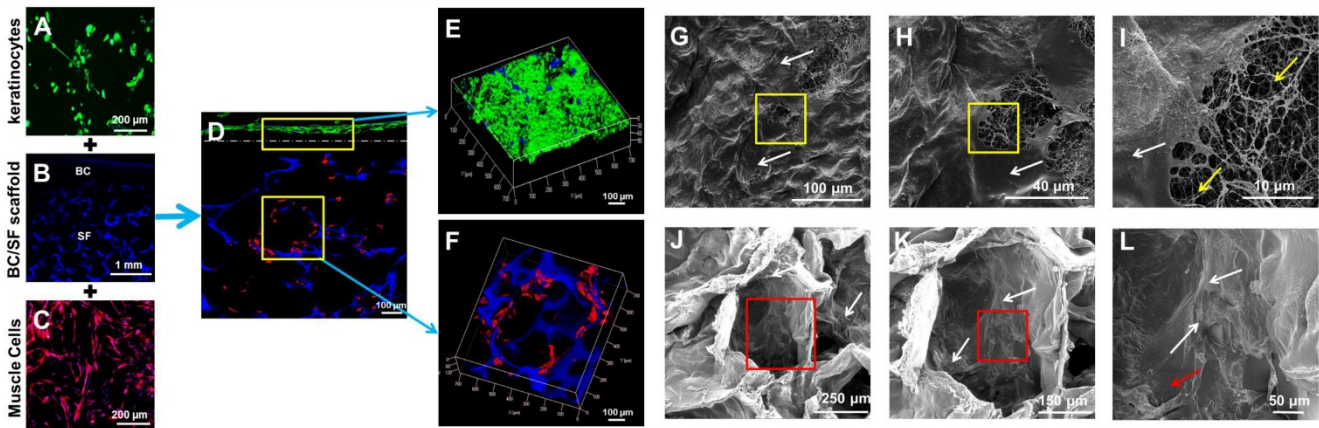


Figure 4. *In vitro* incubation of engineered urethral tissue. (A, C) Immunofluorescence staining of lingual keratinocytes and muscle cells. (B) Immunofluorescence staining of the SF-BC scaffold with DAPI. (D) Immunofluorescence staining of a cross-section of a cell-seeded SF-BC scaffold. (E) Immunofluorescence staining demonstrating that keratinocytes formed a compact confluent keratinocyte layer. (F) Immunofluorescence staining demonstrating that muscle cells invaded the SF-BC scaffold and dispersed throughout the porous polymer. (G-I) SEM analysis of keratinocytes on the compact surface of the SF-BC scaffold. (J-L) SEM analysis of muscle cells located inside the porous network that had grown along the SF wall. The white arrow indicates the cells, the yellow arrow indicates the nanofiber and the red arrow indicates the SF.

Immunofluorescence staining demonstrated that well-defined lingual keratinocytes formed with minimal cellular penetration (Fig. 4 D, E) and the keratinocytes on the compact surface of the SF-BC scaffolds formed a compact confluent keratinocyte layer, which acts as an important barrier. On the opposite side, muscle cells invaded the SF-BC composite scaffolds and dispersed throughout the porous polymer (Fig. 4 D, F).

We further characterized the adhesion of keratinocytes on the compact surface of the SF-BC composite by SEM. The dense network of fibers and small pore size of the pure BC scaffolds directed cell growth to form a compact barrier (Fig. 4 G-I). In contrast, SEM analysis illustrated that muscle cells were inside the porous network and had grown along the SF wall (Fig. 4 J-L), which indicates that SF may provide better guidance for the direction or spacing of cell growth.

Surgical outcomes and follow-up

All animals survived the duration of the study with no adverse events. There were no oral complications, such as difficulty in eating, bleeding, or hematoma, during the three-month period.

At 1 month, retrograde urethrograms showed a wide urethral caliber without a fistula or stricture in group A (Fig. 5 G). All the animals regained satisfactory voiding function in one month without a catheter after the operation. However, group B revealed mild strictures in all dogs, and bladder distension occurred after catheter removal in 3 dogs at 1 month (Fig. 5 I).

At 3 months, retrograde urethrography revealed the maintenance of a wide urethral caliber without any sign of strictures in group A (Fig. 5 H). All the

dogs could urinate without dilation or other treatments. In all dogs in group B, progressive postoperative narrowing of the urethra and bladder distension occurred (Fig. 5 J). There was an obvious difference in success rate between group A and B.

Histological assays were performed on all groups at 1 and 3 months post-operation. At 1 month, all canines in group A had intact epithelial cellular layers: 2-3 layers of well-developed, stratified epithelium (Fig. 6 A, C) and increased numbers of organized muscle bundles were observed (Fig. 6 B, D). In group B, a discontinued epithelium occurred on the lumen surface of the retrieved urethra (Fig. 6 K, M): no muscle fiber bundles were observed (Fig. 6 L, N) and mild chronic inflammatory reactions were characterized by mononuclear cell infiltrates (Fig. 6 K, L). At 3 months, the lumen surface formed intact and multilayer epithelium (Fig. 6 F, H), and large numbers of organized muscle bundles were observed in group A (Fig. 6 G, I). We observed similar epithelium regeneration in group B (Fig. 6 P, R), with little inflammation in the sub-epithelium and small amounts of unorganized muscle fiber bundles (Fig. 6 Q, S). At 1 and 3 months, a large amount of new growth vascular formation was observed in groups A and B (Fig. 6 E, J, O, T).

Discussion

The scaffold is one of the most critical components in tissue engineering because it should provide a temporary structure and milieu for regeneration. The ideal scaffold for the regeneration of a urethra needs to fulfill specific requirements pertaining to the three-dimensional architecture, the environmental needs of the various cell types of the urethra, and provide the diffusion barrier function

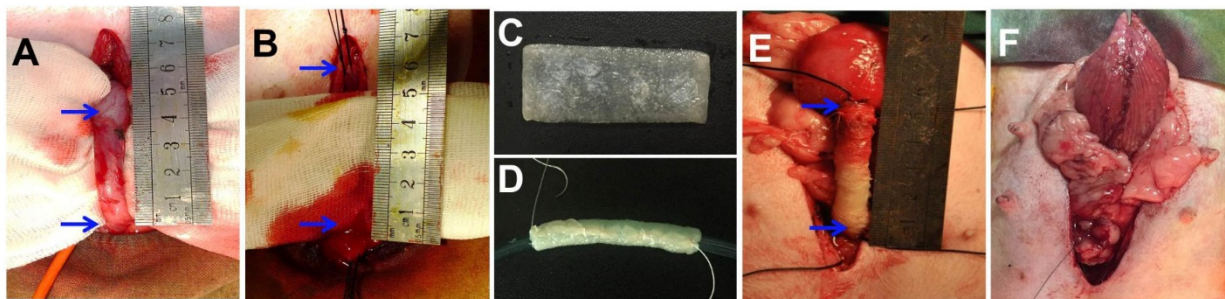
and structural integrity of the urethra. Toward this goal, we have developed a novel technique to manufacture a bilayer scaffold that combines a microporous silk fibroin with a nanofibrous bacterial cellulose scaffold for urethral reconstruction.

BC combines the important and well-known qualities of cellulose with the outstanding features of nanoscale materials [18, 33]. However, BC is less suitable for specific biomedical applications when serving as an implantable scaffold because of its compact nanotextured surface, which lacks a 3-D microenvironment [34]. Our previous studies [35] have demonstrated that SF has potential for use in urethral reconstruction. Plasticity in terms of the silk processing methods allows for the construction of a variety of configurations, including films, foams, hydrogels, gel-spun matrices, and woven or nonwoven meshes. The freeze-drying method might be an appropriate technique because it can create three dimensions and a highly porous scaffold [36], while lacking a nanotextured surface. In our study, a facile and effective method was used to fabricate a nanotextured surface with a microporous (SF-BC) scaffold via stationary cultivation of *Gluconacetobacter xylinus* using an SF microporous scaffold as a template. This bilayered hybrid scaffold combines the advantages of the two materials used.

The scaffold in our study contained a nanotextured BC layer and a microporous SF layer. SF formed the walls of large pores having diameters of

210.2±117.8 μm. The micron-scale pores allow for cell incorporation, migration, proliferation, transport of nutrients and waste products, and tissue growth into the scaffold [37]. The biocompatibility of the scaffolds was evaluated by SEM, which was used to investigate the morphology of the cells on the scaffolds. The muscle cells were distributed mainly in the pores of the scaffold and were anchored onto the SF (Fig. 4 J-L). The BC nanotextured surfaces comprised a fibrous network for cell adhesion and signaling. The lingual keratinocytes had a flat morphology and clustered on the web of cellulose nanofilaments (Fig. 4 G-I). This is consistent with the findings of previous studies that a porous surface structure inhibits the proliferation of epithelial cells, whereas epithelial cells seeded onto flat surfaces proliferate rapidly [38-40]. All these results indicate that this SF-BC scaffold has good biocompatibility. Furthermore, the biomaterials should provide mechanical support to withstand physiological conditions over an extended period of time. For urethral reconstruction, the biomedical scaffold should be successfully sutured to the urethral tissue, and the suture-retention strength should be greater than 0.8 N to ensure implantation [41]. In the current study, the suture-retention strength of the SF-BC scaffold was 1.37±0.14 N, which was considered adequate for implantation. Overall, the SF-BC scaffold has promising prospects in cell culture and tissue engineering.

Surgical procedure



Follow - up

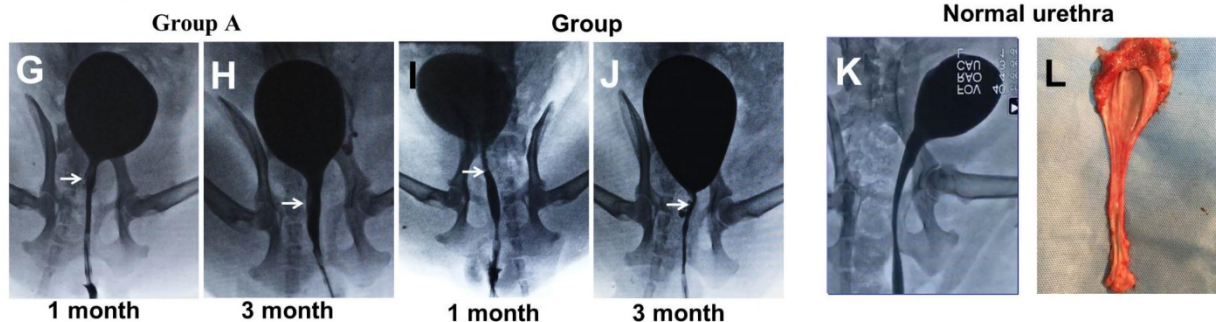


Figure 5. (A-F) During the surgical procedure in a dog model, the urethra between the bladder and the pubic symphysis was exposed, and a 5 cm long urethra section was transected and removed. Then, the scaffold was sutured onto the urethral defect. (G-L) Comparison of urethrography images in each group at 1 and 3 months after operation. The arrow indicates the urethroplasty site of the urethra.

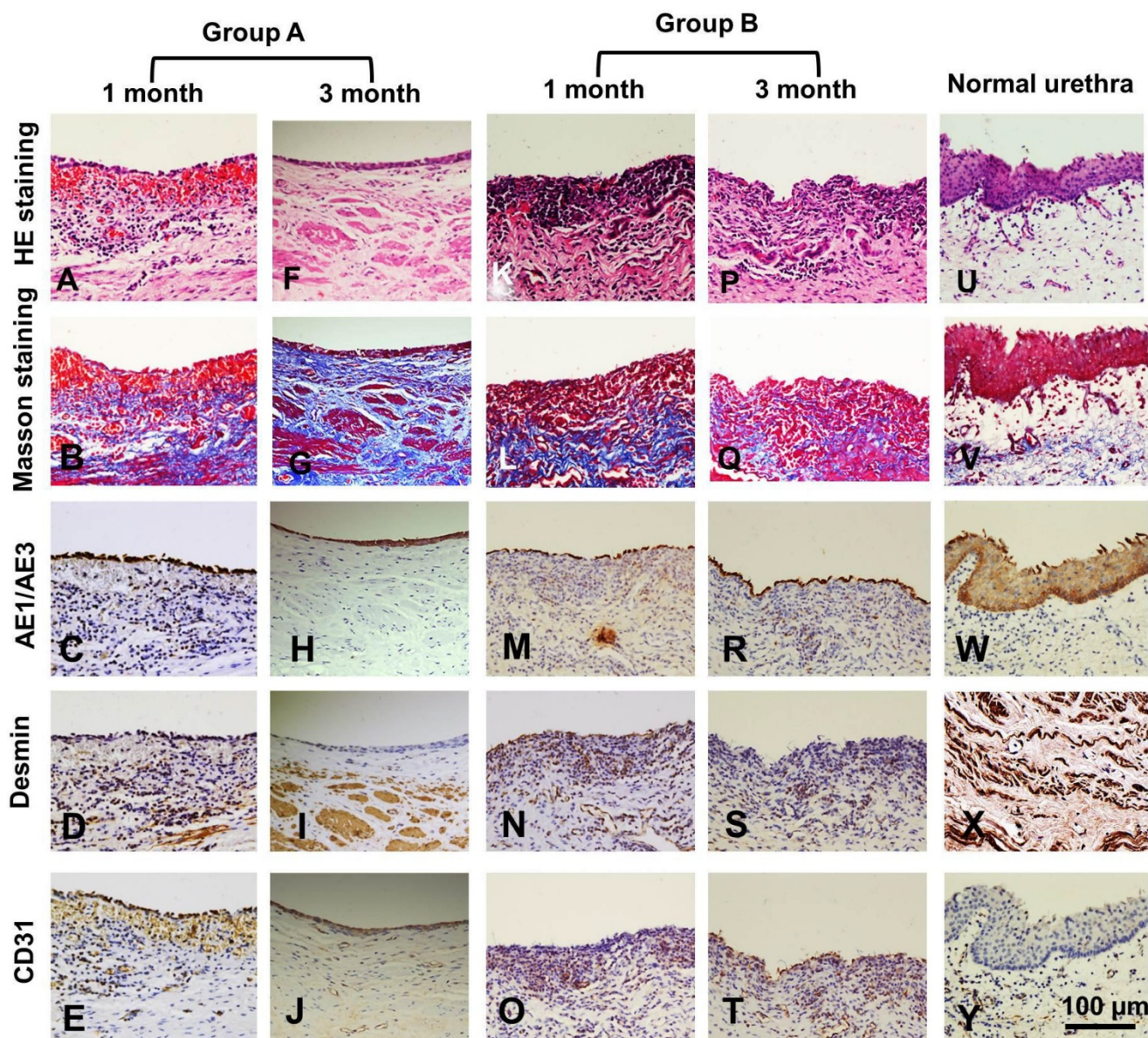


Figure 6. Histologic analysis of reconstructed urethras at one and three months post-implantation. Evaluation of epithelium, smooth muscle and vessels with AE1/AE3, desmin and factor VIII immunohistochemical (IHC) staining in the retrieved urethra; H&E: hematoxylin and eosin.

The maximum defect distance suitable for normal tissue formation using acellular scaffolds that depends on the host cells for tissue regeneration appears to be <1.0 cm [42]. Recent studies indicate that seeding a scaffold with autologous cells can lead to successful repair of urethral defects [43, 44]. Typically, epithelial cells and muscle cells are used to construct TE urethral tissue [45]. Cells obtained from the bladder are a main cell source for cell-based tissue-engineered urethra [26]. However, healthy cells might not be available in patients with chronic inflammation due to urinary tract infections or indwelling catheters. Lingual mucosa are considered the ideal tissue for urethral reconstruction [27]. A previous study demonstrated that lingual keratinocytes and muscle cells can be collected from

the lingual mucosa and used as a source of seed cells for engineering urethral tissue [28]. In the current study, we repaired 5 cm urethral defects using BC-SF scaffolds seeded with lingual keratinocytes and muscle cells in our dog models. SEM revealed that the lingual keratinocytes were stuck tightly onto the SF-BC scaffold with stretching pseudopodially, and lingual keratinocytes expressed AE1/AE3, which is similar to epithelial cells or urothelial cells [9, 46, 47]. These results indicate that lingual keratinocytes had good biocompatibility with the scaffold. The infiltration of muscle cells is critical for the successful regeneration of functional tissue after the implantation of engineered constructs. Atala et al. [45] found that a contributing factor to the success of tubular urethral replacement could be due to the

support provided by a rapidly developing muscle layer that keeps the urethra from collapsing and prevents wall adhesion. Our results also suggest that the regeneration of a suburothelial smooth muscle layer, as observed in group A, provided the optimum muscle orientation and bundle formation.

Vascularization of the graft is necessary to ensure the survival of the implanted tissue. The pore size of a scaffold is closely related to the vascularization of microporous biomaterials implanted *in vivo*. Large pore sizes are beneficial for the growth of blood vessels [48], as we also concluded based on our results. In our study, the number of new blood vessels detected in the SF-BC scaffold with or without cells was high, which indicates the suitability of the SF-BC scaffold for neo-tissue development.

Finally, the experiments described herein focused on the use of this material in the urinary tract. This type of composite scaffold could also be used for numerous other types of hollow-organ tissue engineering grafts, including vascular, bladder, ureteral, esophageal, and intestinal, to provide 3-D bilayer scaffolds with both microporous structures and nanotextured surfaces.

Conclusions

The data presented in this study demonstrate the feasibility of developing 3-D bilayer scaffolds with both microporous structures and nanotextured surfaces via stationary cultivation of *Gluconacetobacter xylinus* using a SF microporous scaffold as a template. The bilayer SF-BC scaffold can provide several advantages and add functionality to the scaffold. The nanotextured BC layer was designed to prevent the erosion of toxic substances in urine and is conducive to the proliferation of epithelial cells. The microporous SF layer was conducive for cells to migrate *in vitro*, and tissue could grow in through the mesh and integrate with surrounding tissues. This study provides preclinical evidence that cell-seeded scaffolds can be used in the reconstruction of urethral defects. More studies are required to establish the feasibility of using the same concept in other biomedical fields.

Abbreviations

SF: silk fibroin; BC: bacterial cellulose; SEM: Scanning electron microscopy; SIS: small intestinal submucosa; BAM: bladder acellular matrix; PLA: polylactic acid; PLGA: poly(lactic-co-glycolic acid); ECM: extracellular matrix; 3D: three-dimensional; TE: tissue-engineered; Micro-CT: microcomputed tomography; PBS: phosphate-buffered saline; DMEM: Dulbecco's modified Eagle's medium; LSM: laser-scanning microscope.KSFM: keratinocyte

serum-free medium; IHC: immunohistochemical; MTT: 3-(4,5-dimethylthiazol-2-yl)-2,5-diphenyltetrazolium bromide; DAPI: 4',6-diamidino-2-phenylindole.

Acknowledgements

This study was supported by National Natural Science Foundation of China (81370795, 51703078 and 81370860), and sponsored by Shanghai Sailing Program(18YF1412800).

Competing Interests

The authors have declared that no competing interest exists.

References

- Chung YG, Tu D, Franck D, Gil ES, Algarrahi K, Adam RM, et al. Acellular bi-layer silk fibroin scaffolds support tissue regeneration in a rabbit model of onlay urethroplasty. *PLoS one*. 2014; 9: e91592.
- Andrich DE, Mundy AR. Substitution urethroplasty with buccal mucosal-free grafts. *J Urol*. 2001; 165: 1131-4.
- Bhargava S, Chapple CR. Buccal mucosal urethroplasty: is it the new gold standard? *BJU Int*. 2004; 93: 1191-3.
- Xu YM, Qiao Y, Sa YL, Zhang J, Fu Q, Song LJ. Urethral reconstruction using colonic mucosa graft for complex strictures. *J Urol*. 2009; 182: 1040-3.
- Jang TL, Erickson B, Medendorp A, Gonzalez CM. Comparison of donor site intraoral morbidity after mucosal graft harvesting for urethral reconstruction. *Urology*. 2005; 66: 716-20.
- Raya-Rivera A, Esquiliano DR, Yoo JJ, Lopez-Bayghen E, Soker S, Atala A. Tissue-engineered autologous urethras for patients who need reconstruction: an observational study. *Lancet*. 2011; 377: 1175-82.
- Horst M, Madduri S, Milleret V, Sulser T, Gobet R, Eberli D. A bilayered hybrid microfibrillar PLGA-acellular matrix scaffold for hollow organ tissue engineering. *Biomaterials*. 2013; 34: 1537-45.
- Xu YM, Fu Q, Sa YL, Zhang J, Song LJ, Feng C. Outcome of small intestinal submucosa graft for repair of anterior urethral strictures. *Int J Urol*. 2013; 20: 622-9.
- Li C, Xu YM, Song LJ, Fu Q, Cui L, Yin S. Urethral reconstruction using oral keratinocyte seeded bladder acellular matrix grafts. *J Urol*. 2008; 180: 1538-42.
- Isotalo T, Tammela TL, Talja M, Valimaa T, Tormala P. A bioabsorbable self-expandable, self-reinforced poly-L-lactic acid urethral stent for recurrent urethral strictures: a preliminary report. *J Urol*. 1998; 160: 2033-6.
- Selim M, Bullock AJ, Blackwood KA, Chapple CR, MacNeil S. Developing biodegradable scaffolds for tissue engineering of the urethra. *BJU Int*. 2011; 107: 296-302.
- Gomez P, 3rd, Gil ES, Lovett ML, Rockwood DN, Di Vizio D, Kaplan DL, et al. The effect of manipulation of silk scaffold fabrication parameters on matrix performance in a murine model of bladder augmentation. *Biomaterials*. 2011; 32: 7562-70.
- Hauser S, Bastian PJ, Fechner G, Muller SC. Small intestine submucosa in urethral stricture repair in a consecutive series. *Urology*. 2006; 68: 263-6.
- Bolland F, Korossis S, Wilshaw SP, Ingham E, Fisher J, Kearney JN, et al. Development and characterisation of a full-thickness acellular porcine bladder matrix for tissue engineering. *Biomaterials*. 2007; 28: 1061-70.
- Franco RA, Min YK, Yang HM, Lee BT. Fabrication and biocompatibility of novel bilayer scaffold for skin tissue engineering applications. *J Biomater Appl*. 2013; 27: 605-15.
- Eberli D, Filho LF, Atala A, Yoo JJ. Composite scaffolds for the engineering of hollow organs and tissues. *Methods*. 2009; 47: 109-15.
- Czaja WK, Young DJ, Kawecki M, Brown Jr RM. The future prospects of microbial cellulose in biomedical applications. *Biomacromolecules*. 2007; 8: 1-12.
- Klemm D, Heublein B, Fink HP, Bohn A. Cellulose: fascinating biopolymer and sustainable raw material. *Angew Chem Int Ed Engl*. 2005; 44: 3358-93.
- Fontana J, De Souza A, Fontana C, Torriani I, Moreschi J, Gallotti B, et al. Acetobacter cellulose pellicle as a temporary skin substitute. *Appl Biochem Biotechnol*. 1990; 24: 253-64.
- Klemm D, Schumann D, Udhardt U, Marsch S. Bacterial synthesized cellulose-artificial blood vessels for microsurgery. *Prog in Polym Sci*. 2001; 26: 1561-603.
- Zaborowska M, Bodin A, Backdahl H, Popp J, Goldstein A, Gatenholm P. Microporous bacterial cellulose as a potential scaffold for bone regeneration. *Acta Biomater*. 2010; 6: 2540-7.
- Petersen N, Gatenholm P. Bacterial cellulose-based materials and medical devices: Current state and perspectives. *Appl Microbiol Biot*. 2011; 91: 1277-86.

23. Park WH, Ha WS, Ito H, Miyamoto T, Inagaki H, Noishiki Y. Relationships between antithrombogenicity and surface free energy of regenerated silk fibroin films. *Fiber Polym.* 2001; 2: 58-63.
24. Santin M, Motta A, Freddi G, Cannas M. *In vitro* evaluation of the inflammatory potential of the silk fibroin. *J Biomed Mater Res.* 1999; 46: 382-9.
25. Omenetto FG, Kaplan DL. New opportunities for an ancient material. *Science.* 2010; 329: 528-31.
26. Bodin A, Bharadwaj S, Wu S, Gatenholm P, Atala A, Zhang Y. Tissue-engineered conduit using urine-derived stem cells seeded bacterial cellulose polymer in urinary reconstruction and diversion. *Biomaterials.* 2010; 31: 8889-901.
27. Song LJ, Xu YM, Lazzeri M, Barbagli G. Lingual mucosal grafts for anterior urethroplasty: a review. *BJU Int.* 2009; 104: 1052-6.
28. Mikami H, Kuwahara G, Nakamura N, Yamato M, Tanaka M, Kodama S. Two-layer tissue engineered urethra using oral epithelial and muscle derived cells. *J Urol.* 2012; 187: 1882-9.
29. Zhu M, Wang K, Mei J, Li C, Zhang J, Zheng W, et al. Fabrication of highly interconnected porous silk fibroin scaffolds for potential use as vascular grafts. *Acta Biomater.* 2014; 10: 2014-23.
30. Lv X, Li Z, Chen S, Xie M, Huang J, Peng X, et al. Structural and functional evaluation of oxygenating keratin/silk fibroin scaffold and initial assessment of their potential for urethral tissue engineering. *Biomaterials.* 2016; 84: 99-110.
31. Lv XG, Feng C, Fu Q, Xie H, Wang Y, Huang JW, et al. Comparative study of different seeding methods based on a multilayer SIS scaffold: Which is the optimal procedure for urethral tissue engineering? *J Biomed Mater Res Part B: Applied Biomaterials.* 2016; 104: 1098-108.
32. Moreira S, Silva NB, Almeida-Lima J, Rocha HA, Medeiros SR, Alves C, Jr., et al. BC nanofibres: *in vitro* study of genotoxicity and cell proliferation. *Toxicol Lett.* 2009; 189: 235-41.
33. Yang J, Lv X, Chen S, Li Z, Feng C, Wang H, et al. *In situ* fabrication of a microporous bacterial cellulose/potato starch composite scaffold with enhanced cell compatibility. *Cellulose.* 2014; 21: 1823-35.
34. Backdahl H, Helenius G, Bodin A, Nannmark U, Johansson BR, Risberg B, et al. Mechanical properties of bacterial cellulose and interactions with smooth muscle cells. *Biomaterials.* 2006; 27: 2141-9.
35. Xie M, Xu Y, Song L, Wang J, Lv X, Zhang Y. Tissue-engineered buccal mucosa using silk fibroin matrices for urethral reconstruction in a canine model. *J Surg Res.* 2014; 188: 1-7.
36. Atala A. Regenerative medicine and tissue engineering in urology. *Urol Clin N Am.* 2009; 36: 199-209.
37. Chen G, Ushida T, Tateishi T. Scaffold design for tissue engineering. *Macromol Biosci.* 2002; 2: 67-77.
38. Eberli D, Freitas Filho L, Atala A, Yoo JJ. Composite scaffolds for the engineering of hollow organs and tissues. *Methods.* 2009; 47: 109-15.
39. Schindler M, Ahmed I, Kamal J. A synthetic nanofibrillar matrix promotes *in vivo*-like organization and morphogenesis for cells in culture. *Biomaterials.* 2005; 26: 5624-31.
40. Kundu AK, Gelman J, Tyson DR. Composite thin film and electrospun biomaterials for urologic tissue reconstruction. *Biotechnol Bioeng.* 2011; 108: 207-15.
41. Billiar K, Murray J, Laude D, Abraham G, Bachrach N. Effects of carbodiimide crosslinking conditions on the physical properties of laminated intestinal submucosa. *J Biomed Mater Res.* 2001; 56: 101-8.
42. Dorin RP, Pohl HG, De Filippo RE, Yoo JJ, Atala A. Tubularized urethral replacement with unseeded matrices: what is the maximum distance for normal tissue regeneration? *World J Urol.* 2008; 26: 323-6.
43. Dorin RP, Pohl HG, De Filippo RE, Yoo JJ, Atala A. Tubularized urethral replacement with unseeded matrices: what is the maximum distance for normal tissue regeneration? *World J Urol.* 2008; 26: 323-6.
44. Raya-Rivera A, Esquiliano DR, Yoo JJ, Lopez-Bayghen E, Soker S, Atala A. Tissue-engineered autologous urethras for patients who need reconstruction: an observational study. *Lancet.* 2011; 377: 1175-82.
45. Orabi H, AbouShwareb T, Zhang Y, Yoo JJ, Atala A. Cell-seeded tubularized scaffolds for reconstruction of long urethral defects: a preclinical study. *Eur Urol.* 2013; 63: 531-8.
46. Feng C, Xu YM, Fu Q, Zhu WD, Cui L. Reconstruction of three-dimensional neourethra using lingual keratinocytes and corporal smooth muscle cells seeded acellular corporal spongiosum. *Tissue Eng Part A.* 2011; 17: 3011-9.
47. Xie M, Song L, Wang J, Fan S, Zhang Y, Xu Y. Evaluation of stretched electrospun silk fibroin matrices seeded with urothelial cells for urethra reconstruction. *J Surg Res.* 2013; 184: 774-81.
48. Zeltinger J, Sherwood JK, Graham DA, Müller R, Griffith LG. Effect of pore size and void fraction on cellular adhesion, proliferation, and matrix deposition. *Tissue Eng Part A.* 2001; 7: 557-72.